RSC Advances

Cite this: *RSC Advances*, 2012, **2**, 8281–8285

www.rsc.org/advances

COMMUNICATION

Controlled synthesis of aligned Ni-NiO core-shell nanowire arrays on glass substrates as a new supercapacitor electrode†

Jin Young Kim,*[a] Se-Hee Lee,[b] Yanfa Yan,[c] Jihun Oh[c] and Kai Zhu*[c]

Received 16th May 2012, Accepted 30th July 2012
DOI: 10.1039/c2ra20947k

Aligned Ni-NiO core-shell nanowire arrays on a glass substrate were prepared *via* electrochemical deposition using porous alumina oxide templates. The core-shell nanowire electrodes displayed prominent supercapacitive behaviors. The rate capability of the electrodes depends strongly on the thickness of the NiO shell layers.

Supercapacitors (sometimes called ultracapacitors or electrochemical capacitors) featuring high power density and long cycle life are promising for their potential use for electric vehicles.[1–3] Pseudo-capacitors based on transition metal oxides represent one type of supercapacitors having the potential for high energy densities. Among various oxides, hydrous RuO_2 exhibits the best performance, but the high cost of RuO_2 has hindered its commercial deployment.[4] Therefore, extensive efforts have been made to search for alternative materials, such as Ni, Mn, or Co-based oxides/hydroxides.[5–9] For instance, pseudo-capacitive behaviors of NiO have been investigated intensively due to its low cost and high specific capacitance.[10,11] However, the poor electronic conduction of NiO has limited its use for high power applications. To achieve high power density, it is necessary to construct electrodes with rapid electron/ion transport through the electrode/electrolyte network and fast redox reactions at the electrode/electrolyte interface. At present, research efforts towards developing high power pseudo-capacitors have been largely focused on the development of nanostructured materials with random structural arrangements, which usually lead to inadequate charge conduction, limiting the rate capability of electrodes. Recently, hybrid electrodes incorporating both metal oxide-based pseudo-capacitor materials and a conductive matrix such as nanoporous gold[12] and various carbon materials[13–15] have shown improved performances by enhancing the electronic conductivity of the electrode materials. In this study, we describe the use of aligned arrays of Ni-NiO core-shell nanowires (NWs) on a charge-conducting substrate (or current collector) as supercapacitor electrodes. Such a Ni–NiO structure has several features that are suitable for supercapacitor applications. The aligned Ni cores provide direct pathways for electron conduction. The oriented pore space surrounding Ni–NiO NWs provide straight open channels for ion conduction. Such an electrode architecture could also avoid the use of either polymer binders or additional conductive additives.

One of the versatile approaches to fabricate aligned NW arrays is to fill up a porous one-dimensional template such as anodized aluminum oxide (AAO) *via* electrochemical deposition.[16,17] The NW arrays are usually prepared using a freestanding AAO layer with one side covered by noble metals (*e.g.*, gold). However, with this approach it is challenging to reproducibly fabricate a physically stable electrode due to the difficulties in handling the brittle ceramic thin layers. Thus, it is preferred that the NWs are grown (with the aid of AAO templates) directly on a conducting substrate. To date, fabrication of such electrodes has only been demonstrated by a few groups for other applications.[18–20]

Here, we demonstrate a facile and reproducible strategy for preparing aligned Ni-NiO core-shell NW arrays directly on a transparent conducting oxide (TCO) substrate. The Ni-NiO core-shell NW electrode displayed pseudo-capacitive behavior, good rate capability and stable cycling performance. The effects of shell thickness on the capacitance and charge/discharge kinetics of supercapacitors are also discussed.

Fig. 1 schematically illustrates the procedure for fabricating aligned Ni-NiO core-shell NW arrays on a TCO substrate. Firstly, a transparent thin AAO template layer (1.9 μm) was prepared by anodizing a thin Al film on a TCO substrate (Fig. 1a). A thin adhesion layer (Ti) and a sacrificial layer (W) were used for selectively removing the bottom (or barrier) oxide layer of the pores of the AAO template.[20] Thus, the electrical contact at the substrate is exposed to the precursor electrolyte during the electrodeposition of Ni NWs. A two-step anodization process was used to produce more ordered AAO pore arrays compared to a single step anodization process.[21,22] The Ni NW arrays were grown by potentiostatically depositing Ni in the pores of AAO using an aqueous solution known as a Watt solution (Fig. 1b).[20] After the Ni deposition, the AAO template was dissolved by an aqueous NaOH solution (Fig. 1c), and then a $Ni(OH)_2$ shell layer was deposited on the surface of Ni NWs *via* galvanostatic deposition in aqueous $Ni(NO_3)_2$ solution.[11] The thickness of $Ni(OH)_2$ was controlled by varying its deposition time.

[a]*Korea Institute of Science and Technology, Photo-electronic Hybrids Research Center, Seoul, 136-791, South Korea. E-mail: kimjy@kist.re.kr; Fax: +82 2 958 6649; Tel: +82 2 958 5368*
[b]*Department of Mechanical Engineering, University of Colorado at Boulder, Boulder, Colorado, 80309, USA*
[c]*National Renewable Energy Laboratory, 1617 Cole Blvd, Golden, CO, 80401, USA. E-mail: Kai.Zhu@nrel.gov; Fax: +1 303 384 6150; Tel: +1 303 384 6353*

† Electronic Supplementary Information (ESI) available: experimental details, SEM image of an AAO template prepared by using a single-step anodization, and SEM image of an AAO template prepared by using a two-step anodization with a 10-minute first-step anodization. See DOI: 10.1039/c2ra20947k

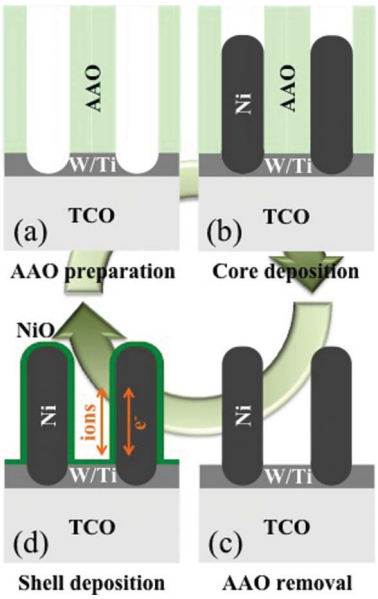

Fig. 1 Schematic illustrations of the (a) AAO template prepared on a TCO substrate, (b) AAO template partially filled with Ni, (c) aligned Ni NW arrays after dissolving the AAO template, and (d) Ni-NiO core-shell NW arrays after $Ni(OH)_2$ deposition and subsequent thermal annealing.

$Ni(OH)_2$ layer was subsequently converted to NiO by thermal annealing at 300 °C for 1 h in air, resulting in the formation of Ni-NiO core-shell NW arrays (Fig. 1d).[23]

Fig. 2 displays the SEM images of the AAO template, Ni core NW arrays, and Ni-NiO core-shell NW arrays. The AAO layer is composed of modestly ordered pores (Fig. 2a). In this study, Al thin films were anodized for a short period of time (*ca.* 4 min) during the first step of the anodization process due to the limited thickness of the thin Al film. This led to the formation of a relatively less ordered pore structure. The polygonal shape of pore openings, which is different from often observed circular shape, seems to be associated with the less ordering of pores. The thickness of the resulting AAO template was about 1.5 μm. It is worth noting the following two

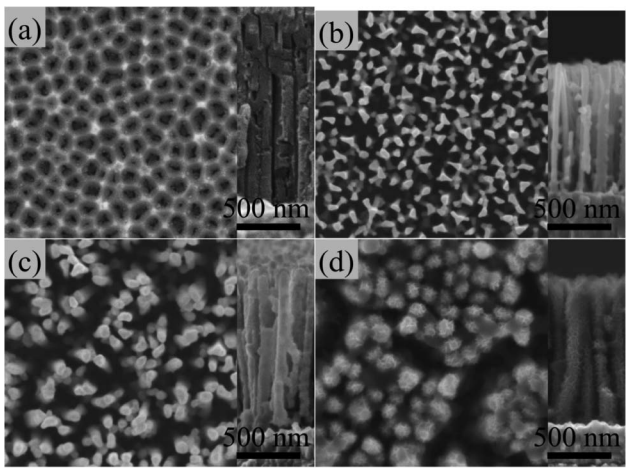

Fig. 2 Top-view and cross-sectional SEM images of the (a) AAO template, (b) Ni core NW arrays, Ni-NiO core-shell NW arrays with either (c) a thinner (deposition charge: 150 mC cm^{-2}) or (d) a thicker (deposition charge: 450 mC cm^{-2}) NiO shell layer.

observations. (1) The extent of pore ordering in the two-step anodized AAO template was improved compared to the single step anodized counterpart (Fig. S1, ESI†). (2) The pore ordering can be further improved if one anodizes the initial sacrificial AAO layer for a longer time (*e.g.*, 10 min) during the first step (Fig. S2, ESI†). Fig. 2b shows the Ni core NW arrays prepared by filling up the pores of the AAO template *via* electrochemical deposition. As expected, the shape of the NW top surface is similar to that of the AAO pore openings. The cross-sectional image shows that the Ni NWs are vertically aligned and well separated. The conformal NiO shell layers were deposited on the Ni NW surface by depositing $Ni(OH)_2$ followed by thermal annealing (Fig. 2c,d). The thicknesses of the shell layers were adjusted by varying the total amount of charges used during the $Ni(OH)_2$ deposition. The deposition was stopped at 150 mC cm^{-2} for a thinner shell layer (Fig. 2c), whereas the deposition was stopped at 450 mC cm^{-2} for a thicker shell layer (Fig. 2d). More interestingly, the NiO shell layer deposited with a total charge of 150 mC cm^{-2} appears relatively dense, whereas the shell layer with an increased deposition charge (450 mC cm^{-2}) exhibits flake-like morphology (Fig. 2d). The flake-like morphology has been observed for NiO thin films deposited using a similar electrodeposition technique.[24] For supercapacitor applications, the Ni cores would be the electron conductor (or collector) and the vertically aligned open pores would serve as the pathways for ion conduction. Therefore, the shell layer thickness/morphology and/or the pore volume are expected to affect the electrode properties, which will be discussed in connection with the results of the electrochemical analyses.

The bright field TEM image in Fig. 3a shows that the Ni NWs have an average diameter of about 60 nm. The distinct contrast in the single wire indicates that the NWs are composed of multiple grains. The convergent beam electron diffraction pattern (upper right in Fig. 3a) and the strong Ni peak in the energy dispersive X-ray spectroscopy (EDS; lower right in Fig. 3a) spectrum indicate that the NW is metallic Ni with a faced centered cubic (fcc) structure. A small peak of oxygen (*ca.* 14 at%) is a result of the surface oxidation during the AAO dissolution and sample preparation. Fig. 3b shows the representative morphology of the Ni-NiO core-shell NWs with a thinner shell layer (corresponding to 150 mC cm^{-2}), where the insets on the right show the EDS spectra obtained from the spots as identified with the corresponding numbers. The measured thickness of the NiO shell layer is 14 nm (*cf.* the deposition charge of 150 mC cm^{-2}). The atomic ratios of Ni to O (*i.e.* Ni/O) calculated from the EDS spectra obtained from spots 2 (core) and 3 (shell) are 2.03 and 0.92, respectively. The Ni/O ratio of about 1 at the shell layer (spot 3) indicates that the shell layer consists of NiO, whereas a higher Ni content is observed at the core (spot 2), resulting from the collective signals from both Ni core and NiO shell. These results confirm that the Ni core NWs are covered by the NiO shell layers. With a longer deposition time (corresponding to 450 mC cm^{-2}), a thicker NiO shell is deposited (Fig. 3c). The bright field TEM image shows that the thickness of the NiO shell layer is 45 nm, which is 3-fold thicker than the thinner shell layer (14 nm; Fig. 3b). Thus, controlling the deposition charge during the electrochemical deposition seems to be an effective approach for adjusting the thickness of the NiO shell layer. The Ni/O ratios calculated from the EDS spectra (3.55 from the core at spot 4 and 1.00 from the shell at spot 5) confirm that the Ni NWs are covered by NiO, as in the case for the thin-shell NWs.

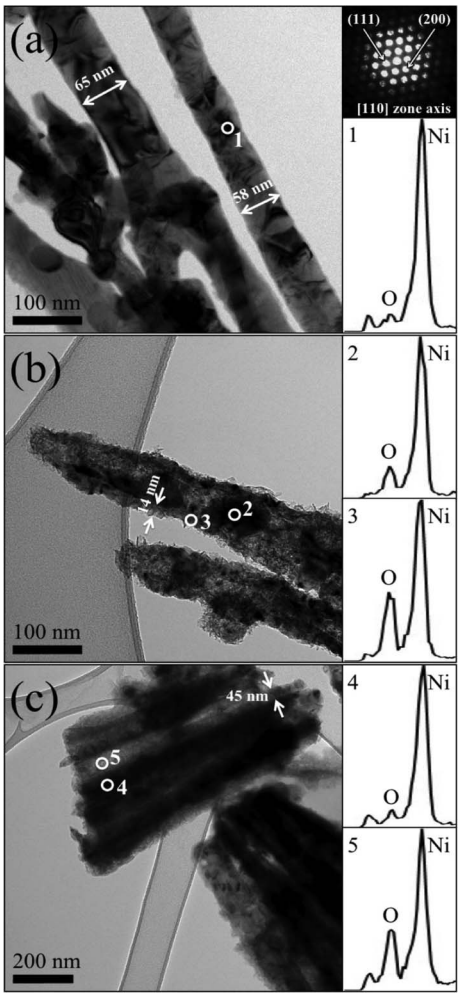

Fig. 3 TEM images of (a) Ni core NWs, (b) Ni-NiO core-shell NW arrays with thinner NiO shell layers (deposition charge: 150 mC cm^{-2}), and (c) Ni-NiO core-shell NW arrays with thicker NiO shell layers (deposition charge: 450 mC cm^{-2}). Insets of (a) show a convergent beam diffraction pattern along [110] direction (upper right) and EDS spectrum (lower right) obtained from the spot identified with a white circle in the TEM image. Insets of (b) and (c) show the EDS spectra obtained from the spots with white circles in the respective TEM images. The EDS spectra are normalized by the maximum intensity of Ni peaks (0.85 keV) and presented in the range of 0 to 1.2 keV.

Fig. 4 shows the electrochemical characteristics of the Ni-NiO core-shell NW electrodes with different shell-layer thicknesses. Fig. 4a shows the cyclic voltammograms (CVs) of the core-shell NWs with a relatively thick shell layer (45 nm, 450 mC cm^{-2}) at scan rates from 2 to 100 mV s^{-1}. The corresponding morphological images of the core-shell NW arrays can be found in Fig. 2d and Fig. 3c. The CV curves show a typical supercapacitive behavior for NiO materials[10,11] as described by the following reversible redox reaction:

$$NiO + OH^- \leftrightarrow NiOOH + e^- \quad (1)$$

Even though the core-shell NW arrays exhibit a capacitive behavior, the current response is voltage-dependent in contrast to the voltage-independent current response for an ideal capacitor. Due to the voltage-dependent current response of the core-shell NW electrodes, the average specific capacitance is calculated by measuring half of the integrated area of the CV curve and then dividing it by the mass of the NiO shell layer. All the CV curves are quite symmetric, implying good reversibility of the redox reaction (eqn (1)). However, the shape of CV curves changes significantly with increasing scan rates; a large shift of the reduction peak with an increasing scan rate is evident (Fig. 4a). This result indicates that the charge/discharge kinetics are not rapid enough at high scan rates for electrodes with thick shell layers. On the other hand, the Ni-NiO NW electrodes with thinner NiO layers (14 nm, 150 mC cm^{-2}; Fig. 3d) exhibit essentially no change in the shape of CV curves (Fig. 4b) for the entire range of scan rates (*i.e.*, 2–100 mV s^{-1}), indicating that the charge/discharge kinetics for NWs with thinner shell layers are rapid enough even at a scan rate of 100 mV s^{-1}. It is noteworthy that at low scan rates ($\leqslant$10 mV s^{-1}), the shape of CV curves for the Ni-NiO NW electrode with a thick NiO layer resembles that for the electrode with a thin NiO layer, suggesting that the same redox reaction (eqn (1)) occurs in both electrodes.

Fig. 4c compares the rate capability of the Ni-NiO core-shell NW electrodes with different shell-layer thicknesses. The specific capacitance was obtained from the CV curves (Fig. 4a,b) and the amount of the active material (*i.e.* NiO) was calculated based on the total amount of charges used for the shell-layer deposition using a conversion constant of 470 μg per 1 C cm^{-2}.[11] It is worth noting that the capacitance of the Ni cores (after thermal annealing) are insignificant compared to that of the electrochemically deposited $Ni(OH)_2$ followed by thermal annealing.[25] The specific capacitance of the core-shell NW arrays with thin NiO shell layers decreases by 27% at the highest scan rate (100 mV s^{-1}) compared to that at the lowest scan rate (2 mV s^{-1}), whereas the thick-shell counterparts show a decrease of 53%. In general, the decreased charge storage capacities with faster charge/discharge rates are attributable to the kinetic limitations inherent in one or more of the three basic steps associated with the redox reaction (eqn (1)): (i) electron transport within the electrode material, (ii) ion diffusion in the electrolyte, and (iii) redox reaction at the electrode/electrolyte interface. Based on the scan-rate dependence of CVs (Fig. 4a,b) and the morphologies of the Ni-NiO NWs (Fig. 2c,d), we attribute the enhanced rate compatibility for the electrode with a thinner NiO layer thickness to the higher electron transport rate across the thinner NiO layer and/or to the faster ion diffusion through the wider pore space between NWs. The specific capacitance values of both samples (141 and 179 F g^{-1} at 10 mV s^{-1} for electrodes with thin and thick NiO shell layers, respectively) are in agreement with those reported for other NiO electrodes.[5,23,24,26] It is worth noting that the Ni-NiO core-shell NW electrode with thinner NiO shell layers has a smaller specific capacitance than the one with thicker NiO layers. This can be understood in connection with their respective morphologies (Fig. 2c,d), *i.e.*, the thicker coating of NiO layer shows a porous flake-like microstructure whereas the thinner NiO layer shows a relatively dense microstructure. The flake-like morphology of NiO supercapacitors would facilitate a higher degree of accessibility for OH^- in the electrolyte to the active NiO material (or, equivalently, a larger effective surface area) and therefore a larger specific capacitance.[12,27]

Fig. 4d shows that the Ni-NiO core-shell NW electrode maintains more than 80% of its initial capacitance after 2000 cycles of galvanostatic charging/discharging processes. In addition, the shapes

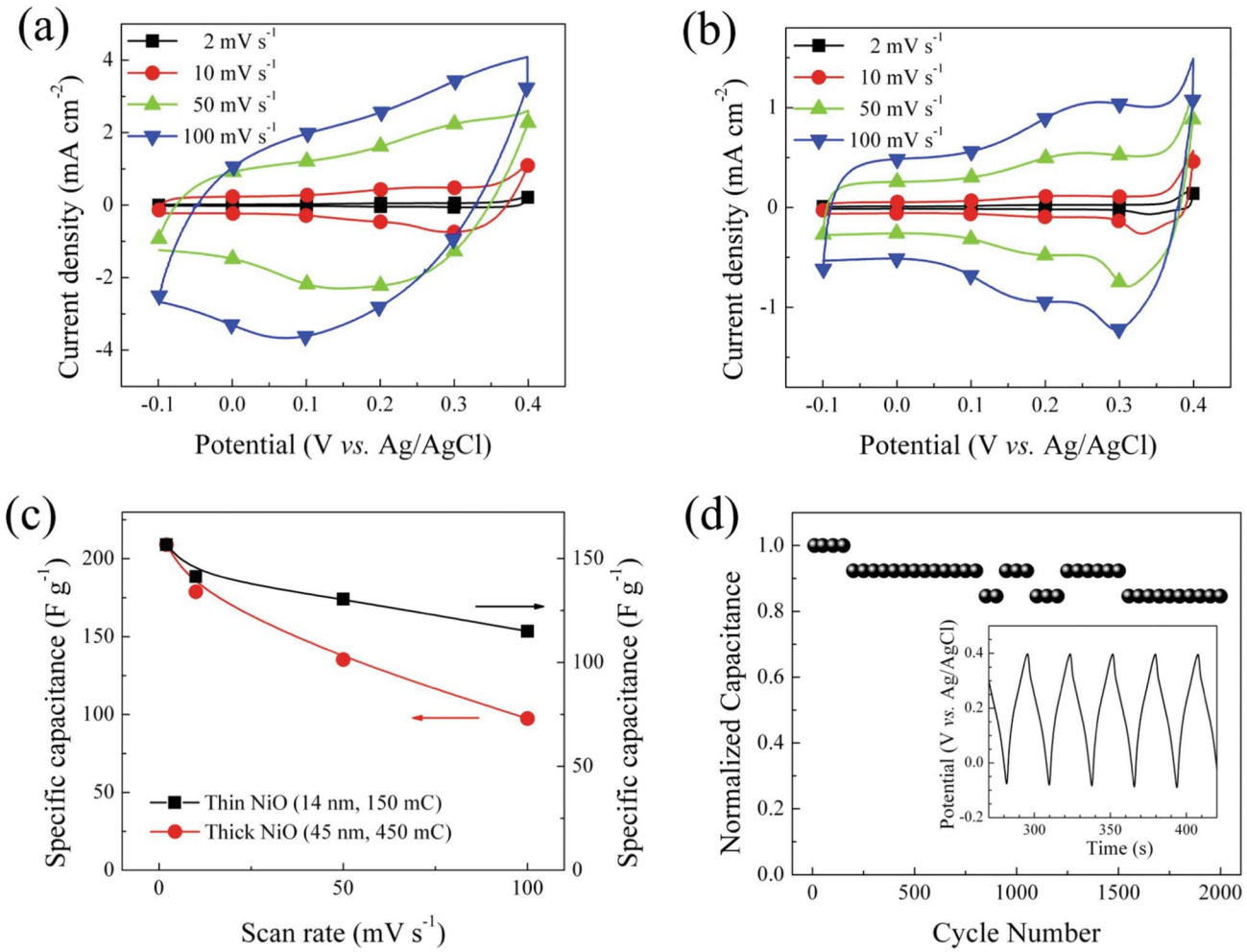

Fig. 4 Cyclic voltammograms of the Ni-NiO core-shell NW arrays with (a) thick NiO shell layers (45 nm, 450 mC cm^{-2}) and (b) thin NiO shell layers (14 nm, 150 mC cm^{-2}). (c) Specific capacitance of the Ni-NiO core-shell NW arrays as a function of the scan rate. (d) Cycle performance of the Ni-NiO core-shell NW arrays at a constant current density (2 mA cm^{-2}); the inset shows typical voltage profiles during the charging/discharging cycling.

of the voltage profiles during the cycling test (inset of Fig. 4d) appeared unchanged during the entire cycling with a coulombic efficiency close to 100%, implying that the microstructure and crystallographic properties of the Ni–NiO NW electrode are stable during the charging/discharging cycles. It should be noted that the supercapacitor performance (capacitance and rate capability) is expected to be further improved by adjusting the density of NWs and/or the dimensions of both the core and the shell layers. For example, thin Ni cores are desired for minimizing the volume fraction of the inactive materials as long as they could provide adequate electronic conductivity. Also, the length of NWs could, in principle, be increased without sacrificing the electronic/ionic conductivities, leading to higher capacitances with similar rate capabilities.

Conclusions

In summary, aligned Ni-NiO core-shell NW arrays were prepared directly on a TCO substrate by using electrochemical deposition with the aid of an AAO template. The bottom layer of the vertically aligned pores of the AAO template could be selectively removed by using a sacrificial W layer, which was essential for the successful electrochemical deposition of aligned Ni NW arrays directly onto the TCO substrate. The SEM and TEM images confirmed the conformal coating of NiO shell layers on the surface of the Ni core NW arrays. The Ni-NiO core-shell NW electrode exhibited super-capacitive behaviors with a specific capacitance of 140–179 F g^{-1} at 10 mV s^{-1}. They also displayed good cycle performance and rate capability. Interestingly, the Ni-NiO NW electrode with a thinner NiO shell layer showed better rate capability than that with a thicker shell layer. These results suggest that the aligned Ni-NiO core-shell NW architecture can be a promising electrode architecture for supercapacitors. The knowledge gained from this study should be valuable in the development of other ordered nanostructures for supercapacitors and other electrochemical applications.

Acknowledgements

This work was supported by the program of Korea Institute of Science and Technology (KIST) and the New & Renewable Energy Technology Development Program of the Korea Institute of Energy Technology Evaluation and Planning (KETEP) grant funded by the Korea government Ministry of Knowledge Economy (No. 20113020010040). This work was also

supported by the U.S. Department of Energy/National Renewable Energy Laboratory's Laboratory Directed Research and Development (LDRD) program under Contract No. DE-AC36-08GO28308.

References

1 J. R. Miller and P. Simon, *Science*, 2008, **321**, 651–652.
2 P. Simon and Y. Gogotsi, *Nat. Mater.*, 2008, **7**, 845–854.
3 J. R. Miller, R. A. Outlaw and B. C. Holloway, *Science*, 2010, **329**, 1637–1639.
4 J. P. Zheng, P. J. Cygan and T. R. Jow, *J. Electrochem. Soc.*, 1995, **142**, 2699–2703.
5 V. Srinivasan and J. W. Weidner, *J. Electrochem. Soc.*, 1997, **144**, L210–L213.
6 M. Toupin, T. Brousse and D. Belanger, *Chem. Mater.*, 2004, **16**, 3184–3190.
7 L. Cao, M. Lu and H. L. Li, *J. Electrochem. Soc.*, 2005, **152**, A871–A875.
8 L. Cao, L. B. Kong, Y. Y. Liang and H. L. Li, *Chem. Commun.*, 2004, 1646–1647.
9 L. Cao, F. Xu, Y. Y. Liang and H. L. Li, *Adv. Mater.*, 2004, **16**, 1853.
10 K. C. Liu and M. A. Anderson, *J. Electrochem. Soc.*, 1996, **143**, 124–130.
11 K. W. Nam and K. B. Kim, *J. Electrochem. Soc.*, 2002, **149**, A346–A354.
12 J. W. Lang, L. B. Kong, W. J. Wu, Y. C. Luo and L. Kang, *Chem. Commun.*, 2008, 4213–4215.
13 X. P. Dong, W. H. Shen, J. L. Gu, L. M. Xiong, Y. F. Zhu, Z. Li and J. L. Shi, *J. Phys. Chem. B*, 2006, **110**, 6015–6019.
14 K. W. Nam, E. S. Lee, J. H. Kim, Y. H. Lee and K. B. Kim, *J. Electrochem. Soc.*, 2005, **152**, A2123–A2129.
15 H. L. Wang, H. S. Casalongue, Y. Y. Liang and H. J. Dai, *J. Am. Chem. Soc.*, 2010, **132**, 7472–7477.
16 Y. K. Zhou, C. M. Shen and H. L. Li, *Solid State Ionics*, 2002, **146**, 81–86.
17 H. X. Ji, J. S. Hu, Y. G. Guo, W. G. Song and L. J. Wan, *Adv. Mater.*, 2008, **20**, 4879.
18 M. L. Tian, S. Y. Xu, J. G. Wang, N. Kumar, E. Wertz, Q. Li, P. M. Campbell, M. H. W. Chan and T. E. Mallouk, *Nano Lett.*, 2005, **5**, 697–703.
19 K. P. Musselman, G. J. Mulholland, A. P. Robinson, L. Schmidt-Mende and J. L. MacManus-Driscoll, *Adv. Mater.*, 2008, **20**, 4470–4475.
20 J. Oh and C. V. Thompson, *Adv. Mater.*, 2008, **20**, 1368.
21 H. Masuda and M. Satoh, *Jpn. J. Appl. Phys.*, 1996, **35**, L126–L129.
22 W. Lee, H. Han, A. Lotnyk, M. A. Schubert, S. Senz, M. Alexe, D. Hesse, S. Baik and U. Gosele, *Nat. Nanotechnol.*, 2008, **3**, 402–407.
23 K. W. Nam, W. S. Yoon and K. B. Kim, *Electrochim. Acta*, 2002, **47**, 3201–3209.
24 K. R. Prasad and N. Miura, *Appl. Phys. Lett.*, 2004, **85**, 4199–4201.
25 J. H. Kim, S. H. Kang, K. Zhu, J. Y. Kim, N. R. Neale and A. J. Frank, *Chem. Commun.*, 2011, **47**, 5214–5216.
26 J. H. Kim, K. Zhu, Y. F. Yan, C. L. Perkins and A. J. Frank, *Nano Lett.*, 2010, **10**, 4099–4104.
27 C. Z. Yuan, X. G. Zhang, L. H. Su, B. Gao and L. F. Shen, *J. Mater. Chem.*, 2009, **19**, 5772–5777.